Steady Couette flows of elastoviscoplastic fluids are nonunique

I. Cheddadi[a)]

INRIA Paris - Rocquencourt, BANG team, Domaine de Voluceau, Rocquencourt, B.P. 105, 78153 Le Chesnay, France

P. Saramito

Laboratoire Jean Kuntzmann, UMR 5524 Univ. J. Fourier - Grenoble I and CNRS, BP 53, F-38041 Grenoble Cedex, France

F. Graner

BDD, Institut Curie, CNRS UMR 3215 and INSERM U 934, 26 rue d'Ulm, F-75248 Paris Cedex 05, France and Matière et Systèmes Complexes (MSC), UMR 7057 CNRS & Université Paris Diderot, 10 rue Alice Domon et Léonie Duquet, 75205 Paris Cedex 13, France

(Received 27 July 2011; final revision received 3 November 2011; published January 13, 2012)

Synopsis

The Herschel–Bulkley rheological fluid model includes terms representing viscosity and plasticity. In this classical model, below the yield stress the material is strictly rigid. Complementing this model by including elastic behavior below the yield stress leads to a description of an elastoviscoplastic (EVP) material such as an emulsion or a liquid foam. We include this modification in a completely tensorial description of cylindrical Couette shear flows. Both the EVP model parameters, at the scale of a representative volume element, and the predictions (velocity, strain and stress fields) can be readily compared with experiments. We perform a detailed study of the effect of the main parameters, especially the yield strain. We discuss the role of the curvature of the cylindrical Couette geometry in the appearance of localization; we determine the value of the localization length and provide an approximate analytical expression. We then show that, in this tensorial EVP model of cylindrical Couette shear flow, the normal stress difference strongly influences the velocity profiles, which can be smooth or nonsmooth according to the initial conditions on the stress. This feature could explain several open questions regarding experimental measurements on Couette flows for various EVP materials such as emulsions or liquid foams, including the nonreproducibility that has been reported in flows of foams. We then discuss the suitability of Couette flows as a way to measure rheological properties of EVP materials. © *2012 The Society of Rheology*. [DOI: 10.1122/1.3675605]

[a)]Author to whom correspondence should be addressed; electronic mail: ibrahim.cheddadi@inria.fr

I. INTRODUCTION

Localization is a phenomenon often observed in two- or three-dimensional shear flows of complex materials: Coussot *et al*. (2002) observed it for emulsions, Salmon *et al*. (2003a) for colloids, Howell *et al*. (1999), Mueth *et al*. (2000), Losert *et al*. (2000), and Huang *et al*. (2005) for wet granular materials. It consists of a coexistence between a region localized near a moving boundary, where the material flows like a liquid, and another region where the material behaves like a solid.

Since the pioneering experiment of Debrégeas *et al*. (2001) (Fig. 1), liquid foams [gas bubbles dispersed within a continuous liquid phase, as explained by Weaire and Hutzler (1999) and Cantat *et al*. (2010)] have been widely used for experimental, theoretical, and numerical studies of localization [for reviews see, e.g., Höhler and Cohen-Addad (2005); Schall and van Hecke (2010); Barry *et al*. (2011)]. Their discrete units, the gas bubbles, are easy to observe (especially in two dimensions) and to manipulate. Moreover, they display simultaneous elastic, viscous, plastic behaviors (referred to as *elastoviscoplastic* or EVP), thus covering a wide range of behaviors observed in many complex materials.

The aim of this paper is to show that including tensorial elasticity in the classical viscoplastic Herschel–Bulkley (VP) model leads to many improvements in the understanding of Couette flows of nonthixotropic EVP fluids such as emulsions, liquid foams, or carbopol gel. These materials exhibit normal stresses that arise from the local anisotropy (hence, the necessity of a *tensorial* description) of the *elasticity* related to their microstructure. Localization can appear if the material yields, that is, if the material is *plastic*; in the regions below the yield strain, the normal stresses can remain finite even in a steady-state flow. If, in addition, *viscous* dissipation occurs during plastic events, elasticity is coupled to viscosity in the flowing region, so that the normal stresses are coupled to the velocity gradient, even in the Couette geometry.

Cheddadi *et al*. (2008, 2009, 2011a) have previously explored this approach with the Saramito (2007) model (Bingham-like plastic dissipation), for cylindrical Couette flows of liquid foams and other EVP flows around an obstacle; they have successfully explained the observations of normal stresses components measured by Janiaud and Graner (2005) in the experimental data of Debrégeas *et al*. (2001).

In the present work, the theoretical predictions of the Saramito (2009) model are compared with experimental measurements, including shear and normal stresses when

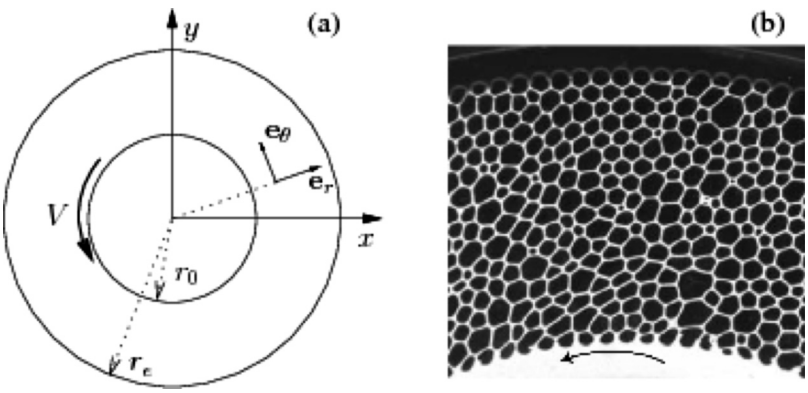

FIG. 1. Experimental setup for a two-dimensional circular shear flow of a foam confined between two horizontal plates. (a) Definition of the geometric and kinematic parameters; (b) picture of the confined two-dimensional liquid foam [from Debrégeas *et al*. Phys. Rev. Lett. 87, 178305, (2001). Copyright © 2001 The American Physical Society: the internal radius is $r_0 = 71$ mm.

available. This model is an extension of the Saramito (2007) model that includes a Herschel–Bulkley-like plastic dissipation.

We study the influence of the dimensionless rheological parameters, including the yield strain and the cylindrical Couette geometry curvature (introduced in Sec. III). For simplicity, we focus here on the low velocity regime corresponding to most published foam Couette flow experiments; we postpone, for future work, analysis of both the quasi-static regime where viscosity plays no visible role, studied in simulations [Wyn *et al*. (2008); Raufaste *et al*. (2010)], and the high velocity regime where viscous and friction effects are dominant [see, e.g., Katgert *et al*. (2008, 2009, 2010)]. The inclusion of elasticity and tensorial descriptions is two essential features of the present modeling, leading to three predictions not captured by scalar and/or VP models. First, we show that normal stresses that depend on the preparation of the material [Labiausse *et al*. (2007)] can persist as residues even in steady flow. Second, we predict that velocity flow profiles are either smooth or nonsmooth depending on the measured value of the stress tensor. Third, as a consequence of these two results, two- and three-dimensional cylindrical Couette flows of EVP materials are nonunique, even in steady state. To summarize, the effect we describe in this paper is not specific to a given material microstructure but is more generally a consequence of the material's visco-elasto-plasticity and of the specifically tensorial nature of the Couette flow.

The outline of the paper is as follows. Section II reviews and discusses the main open questions found in the literature, which we address here. Section III discusses some constitutive equations for EVP materials, in particular, the EVP model of Saramito (2009). Section IV presents the solutions of this model and some of the main features which are absent from VP models: the effect of initial conditions, memory effects, nonuniqueness, and nonsmooth solutions; we also explain how such EVP model can be compared to actual experimental data. Section V examines how variations of the EVP model parameters affect these flow features and provides an approximate analytical expression for the localization length [Eq. (15)]. Section VI discusses the consequences of our results. Section VII summarizes our findings.

II. OPEN QUESTIONS

During the last 10 years there has been extensive debate on the Couette flow of various complex fluids, raising some theoretical questions [see, e.g., Schall and van Hecke (2010)]:

- What is the physical origin of localization?
- Where does the material localize?
- Why do some experiments report smooth profiles at the localization position and some others experiments report nonsmooth ones?

Before we examine the status of these questions, we first need to clarify the vocabulary and hypotheses used in the literature:

- We assume here that the materials of interest can be described using continuum mechanics: this implies that there is a representative volume element (RVE). The RVE should be smaller than the scale of the global flow, but large enough so that one can define: (i) variables such as stresses, strains, and velocity gradient; and (ii) parameters, such as elastic modulus, yield strain, and viscosity. Note that in an EVP material stress, strain and deformation rate are variables which can be independently defined and measured *in situ* if the material can be imaged in full details [Graner *et al*. (2008)].

- Since the phrase "shear banding" [Vermant (2001)] is used to describe different things, we prefer not to use it. We instead use "smooth" (resp: "nonsmooth") to indicate that the velocity gradient is continuous (resp: discontinuous).
- The word "localization" is a historical term used consistently to mean "coexistence of rigid and flowing regions." We thus use it here.
- In cylindrical Couette flows, the localization radius, denoted as r_c, admits several possible definitions [see Gilbreth *et al.* (2006) or Sec. VII C of Weaire *et al.* (2010)]. Here, we choose to define r_c as the position separating the flowing region from the rigid one, or equivalently as the limiting value of the radius at which the deformation rate is zero.
- There are at least two different ways, one in mathematics and one in rheology, used to define the norm of a tensor, and thus the von Mises criterion regarding the yield strain and stress: we choose the mathematical one, presented below [see Eq. (4) and discussion thereafter].

A. What is the physical origin of the localization?

There are several explanations for the origin of the localization; many of them are reviewed and discussed by Schall and van Hecke (2010).

Coussot *et al.* (2002) used nuclear magnetic resonance imaging (MRI) methods to measure the local velocity in three-dimensional cylindrical Couette flows of other EVP materials such as carbopol gel, and more generally yield stress fluids such as bentonite suspensions and cement paste. Despite the apparent simplicity of shear flows, a common description of these experiments is still lacking [see Ovarlez *et al.* (2009) for a review]: on the one hand, thixotropic materials exhibit an intrinsic critical shear rate, i.e., these materials cannot flow homogeneously at a shear rate smaller than a critical value, which is characteristic of the material; on the other hand, nonthixotropic materials may or may not exhibit a critical shear rate (that does not seem to be intrinsic to the material), as discussed in Sec. II C. We focus here on nonthixotropic materials and try to explain this peculiar behavior.

1. *Intrinsic explanations invoking a nonmonotonic constitutive equation*

In complex materials which display a shear-induced structural transition, a possible source of localization is the coexistence of two different shear rates at the same stress, that is, the shear stress versus *shear rate* curve is multivalued [Huseby (1966); Berret *et al.* (1994); Porte *et al.* (1997); Decruppe *et al.* (2001); Bénito *et al.* (2010)]. In fact, foam experiments [Khan *et al.* (1988)] and simulations [Kabla *et al.* (2007); Okuzono and Kawasaki (1995); Raufaste *et al.* (2010)] suggest that in the quasistatic regime the shear stress versus *shear strain* curve passes through an overshoot before reaching a plateau, thus being multivalued [Clancy *et al.* (2006); Weaire *et al.* (2009, 2010)].

This explanation is probably not generally applicable to foams in Couette experiments: foams usually contain at least a few percent liquid, so that their yield strain is lower than for ideally dry foams [Marmottant *et al.* (2008)] and the overshoot becomes undectable [Raufaste *et al.* (2010)]. Moreover, even in theory and simulations of dry foams, the overshoot disappears if the foam is too disordered [Raufaste *et al.* (2010)]. This discussion is beyond the scope of the present paper, where we explore the complex behavior emerging from a simple EVP constitutive equation.

2. *Extrinsic explanations invoking a nonhomogeneous stress*

In the case of a cylindrical Couette geometry, the curvature induces a spatial heterogeneity of the stress, the inner part being above the yield stress and flowing, and the outer

part being below the yield stress and nonflowing [Adams and Olmsted (2009)]. This explanation of localization requires a yield stress, and thus arises in VP and EVP models.

An alternative interpretation has been presented by Wang *et al*. (2006) for two-dimensional foams. They performed experiments with two configurations in a *plane* Couette geometry: either bubbles floating on water (bubble raft) or bubbles confined between water and a glass plate. They observed localization only in the second case, when a glass plate is present. Therefore, the competition between the internal viscosity of the foam and the *external friction* from the glass plates has been suggested by Wang *et al*. (2006) and Janiaud *et al*. (2006) as a possible cause for localization, even in the case of circular geometries [Clancy *et al*. (2006)].

Cheddadi *et al*. (2008) have reconciled these views by comparing in detail the Saramito (2007) EVP model with both steady and transient regimes of the Debrégeas *et al*. (2001) experiment of a two-dimensional foam confined between two glass plates. They have shown that the simple explanation of a nonhomogeneous stress is still valid for such systems. The curvature of flow lines and the friction on the glass plates are only two different possible causes for stress heterogeneity. In practice, the friction of glass plates is so small [Cheddadi *et al*. (2008)] that it plays a visible role only in the absence of flow line curvature, as in the plane geometry of Wang *et al*. (2006). In two-dimensional cylindrical Couette flows, the available data are not compatible with this friction-dominated interpretation and are compatible with the stress heterogeneity that arises from geometry.

In what follows, we neglect the friction on plates, and use two-dimensional foams as model systems for two- or three-dimensional nonthixotropic EVP fluids.

B. What is the localization position r_c?

In cylindrical Couette flows, Weaire *et al*. (2010) have reviewed the dependency of the localization position on the cylinder velocity. They find that in the low velocity regime, it is basically undetermined: there is a range of possible values for the localization position and, moreover, the size of this range diverges when the velocity decreases. There are two questions: is there a hidden variable which fixes the localization position? for a given experiment, is the position predictable?

To answer these questions, in Sec. V, we explicitly determine the localization position, and study its dependence on model parameters and initial conditions.

C. Why smooth and/or nonsmooth profiles?

The first observation of foam Couette flows by Debrégeas *et al*. (2001) reported a *smooth* velocity profile [Fig. 2(a)].

However, in 2002, Coussot *et al*. (2002) observed *discontinuous* shear rate profiles on Couette flows of emulsions and suspensions [Fig. 2(b)]. A discontinuity (denoted $\dot{\gamma}_c$) of the shear rate at $r = r_c$ was measured: so, the velocity profile is nonsmooth at $r = r_c$, since its derivative is related to the shear rate. Such nonsmooth profiles were found by others between 2003 and 2008: for wormlike micelles by Salmon *et al*. (2003a), for lyotropic lamellar systems by Salmon *et al*. (2003b), for Couette foam flows by Lauridsen *et al*. (2004), Gilbreth *et al*. (2006), Dennin (2008), Krishan and Dennin (2008), and interpreted theoretically by Denkov *et al*. (2009), Clancy *et al*. (2006), and Weaire *et al*. (2010).

Surprisingly, in 2008–2010, experiments published by Katgert *et al*. (2008, 2009, 2010), Coussot and Ovarlez (2010), and Ovarlez *et al*. (2010) showed smooth velocity profiles and continuous shear rates at $r = r_c : \dot{\gamma}_c$ equals zero. Note that some papers with contradictory results shared either an author [Coussot *et al*. (2002); da Cruz *et al*. (2002); Huang *et al*. (2005); Coussot and Ovalez, (2010)] or a set-up, the bubble raft [Lauridsen

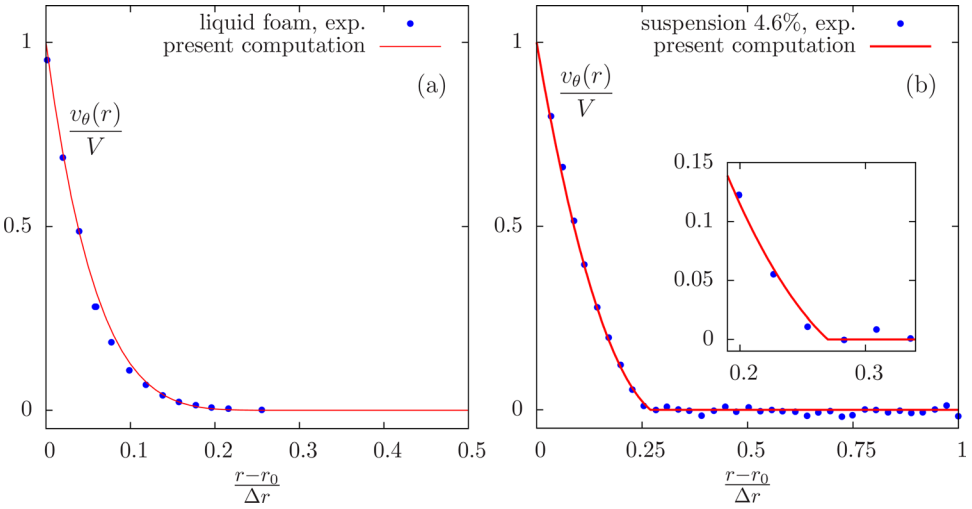

FIG. 2. Smooth and nonsmooth velocity profiles. Experimental data are compared with our computations as discussed in Sec. IV D. (a) Smooth profile: comparison of experimental data on a foam by Debrégeas *et al.* (2001) with the present computations ($\varepsilon_Y = 0.175$, $Bi = 10$, $Co = 0.41803$, $n = 1/3$); (b) nonsmooth profile: comparison of experimental data on a bentonite-water suspension from Fig. 1(a) of Coussot *et al.* (2002), with the present computations ($\varepsilon_Y = 0.35$, $Bi = 27$, $Co = 1/3$, $n = 1$). Inset: zoom around $r = r_c$.

et al. (2004); Gilbreth *et al.* (2006); Dennin (2008); Krishan and Dennin (2008); Katgert *et al.* (2008, 2009, 2010)].

Coussot and Ovarlez (2010) explained this discrepancy by questioning the quality of the experiments: "previous data on a specific foam [Rodts *et al.* (2005)] were probably affected by experimental artifacts." Similarly, Ovarlez *et al.* (2010) explain that "Our measurements demonstrate that three-dimensional foams do not exhibit observable signatures of (discontinuous) shear banding. This contrasts with the results of Rodts *et al.* (2005) and da Cruz *et al.* (2002) which we have shown to pose several experimental problems" and mention that "the case of bubble rafts is still unclear."

Our results emphasize the intrinsic sensitivity of the equations to the sample history [Bénito *et al.* (2010)]; this could explain why experimental artifacts such as impurities [Rodts *et al.* (2005)] or bubble rupture [da Cruz *et al.* (2002)] could yield drastic changes in observations. Even when experimental artifacts are eliminated, our results regarding the effect of trapped stresses due to initial conditions provide a deep reason to explain why, according to the set-up or foam preparation, either a smooth or a nonsmooth profile could appear.

III. CONSTITUTIVE EQUATION

A. Brief review of EVP models

A number of closely related models have appeared in the literature [see Saramito (2007) for a review]. Table I distinguishes models with respect to their behavior before and after yielding, their applicability to three-dimensional general flows, and to the existence of a proof that the dissipation is positive.

We now discuss the mathematical formulation and properties of some of these models. The equations are written in two dimensions with polar coordinates to fit with the cylindrical Couette geometry. Table II lists the corresponding dimensionless parameters. In

TABLE I. Summary of the referenced EVP models. The 3D column is marked when the model has been written in a general tensorial sense, e.g., with objective derivatives. The TH column is also marked when the model has a positive dissipation according to the second law of thermodynamics. The italic mark *X* in the 3D or the TH columns means that the corresponding property was derived after publication of this model. For instance, the Bingham and the Herschel–Bulkley models were first proposed in a one-dimensional simple shear flow context, then extended to three dimensions, and finally found to satisfy the second law of thermodynamics.

Contribution	Before yielding	After yielding	3D	TH
Schwedoff (1900)	Rigid solid	VE fluid		
Bingham (1922)	Rigid solid	Newtonian fluid	*X*	*X*
Herschel and Bulkley (1926)	Rigid solid	Power-law fluid	*X*	*X*
Oldroyd (1947)	Elastic solid	Newtonian fluid	**X**	*X*
Isayev and Fan (1990)	Elastic solid	VE fluid	**X**	**X**
Doraiswamy *et al.* (1991)	Elastic solid	Power-law fluid	**X**	
Puzrin *et al.* (2003)	Elastic solid	VE *solid*	**X**	**X**
Saramito (2007)	VE solid	VE fluid	**X**	**X**
Bénito *et al.* (2008)	VE solid	VE fluid	**X**	**X**
Saramito (2009)	VE solid	Power-law VE fluid	**X**	**X**

each model, the constitutive equation is closed with equations for momentum and mass balance, and appropriate Couette flow boundary and initial conditions. Since external forces and inertia are negligible here [see Sec. II A and Cheddadi *et al.* (2008)], the momentum balance reduces to

$$\nabla \cdot \tau = 0, \tag{1}$$

where τ is the stress tensor. The material is assumed to be incompressible, so the mass balance is

$$\nabla \cdot \mathbf{v} = 0, \tag{2}$$

where $\mathbf{v}$ is the velocity.

B. VP model: Herschel–Bulkley

Herschel and Bulkley (1926) proposed a power-law variant of the viscoplastic Bingham (1922) model [see also Oldroyd (1947)]

TABLE II. Four dimensionless numbers (ε_Y, Bi, Co, n), or equivalently (We, Bi, Co, n), which completely characterize the Saramito (2009) model in the circular Couette geometry.

Symbol	Name	Definition	Physical meaning	Typical range
ε_Y	Yield strain	$\frac{\tau_Y}{2G}$ [Eq. (11)]	Elastoplasticity	[0,0.5]
Bi	Bingham	$\frac{\tau_Y \Delta r}{\eta V}$ [Eq. (5)]	Viscoplasticity	[0,100]
Co	Curvature	$\frac{r_e - r_0}{r_e}$ [Eq. (6)]	Curvature	[0,1]
n	Power-law index	[Eq. (3)]	Shear thinning	[0.3,1]
We	Weissenberg	$\frac{\eta V}{G \Delta r} = \frac{2\varepsilon_Y}{Bi}$ [Eq. (9)]	Viscoelasticity	[0,0.04]

$$\begin{cases} \tau = 2K|D|^{n-1}D + \tau_Y \frac{D}{|D|} & \text{when } |D| \neq 0, \\ |\tau_d| \leq \tau_Y & \text{otherwise,} \end{cases} \tag{3}$$

$$\text{or equivalently: } \max\left(0, \frac{|\tau_d| - \tau_Y}{2K|\tau_d|^n}\right)^{1/n} \tau = D,$$

where $D = (\nabla \mathbf{v} + \nabla \mathbf{v}^T)/2$ is the deformation rate tensor, $|D| = \sqrt{D_{ij}D_{ij}}$ its Euclidian norm, and $(\nabla \mathbf{v})_{ij} = (\partial_j v_i)$ is the velocity gradient tensor. The so-called deviatoric stress τ_d is defined according to the spatial dimension in which the flow is investigated: $\tau_d = \tau - (1/N)I$, where I is the identity matrix, and $N = 1$, 2 or 3. We focus here on two-dimensional flows and take $N = 2$. Here, $\tau_Y > 0$ is the yield stress, $K > 0$ is the consistency parameter, and $n > 0$ is the power-law index.

The von Mises criterion, $|\tau_d| \leq \tau_Y$, involves the Euclidian norm of the deviatoric part of the stress. In cylindrical coordinates, it is written

$$|\tau_d| = \left(2\tau_{r\theta}^2 + \frac{(\tau_{rr} - \tau_{\theta\theta})^2}{2}\right)^{1/2}. \tag{4}$$

Note that, favoring the shear stress, some authors use a slightly different definition of the deviatoric stress norm [Raufaste *et al.* (2010)]: $\left(\tau_{r\theta}^2 + (\tau_{rr} - \tau_{\theta\theta})^2/4\right)^{1/2}$. This rheological definition would lead to an alternative, equivalent model: keeping the same Eq. (3), it would only multiply the deviatoric stress norm $|\tau_d|$ by $2^{-1/2}$, the yield stress τ_Y by $2^{-1/2}$, and the consistency K by $2^{(n-1)/2}$.

In the circular Couette geometry, V denotes the velocity of the inner cylinder and $\Delta r = r_e - r_0$ the width of the gap. Note that $\eta = K(V/\Delta r)^{n-1}$ has the dimension of a viscosity and that $\eta = K$ when $n = 1$. The dimensionless Bingham number is

$$Bi = \frac{\tau_Y \Delta r}{\eta V}. \tag{5}$$

It compares the yield stress τ_Y with a characteristic viscous stress $\eta V/\Delta r$. Let us also introduce the dimensionless number Co

$$Co = 1 - \frac{r_0}{r_e}, \tag{6}$$

that quantifies the curvature of the circular Couette geometry. When the two radii are close, this number is close to zero. Conversely, when the curvature is extreme, e.g., r_0 becomes small, this number tends to one.

The Herschel–Bulkley model predicts localization in the circular Couette geometry, as a result of the stress heterogeneity. Its position r_c can be numerically computed [see Appendix A, Eq. (A1)].

The Herschel–Bulkley model reduces to the Bingham one when $n = 1$, to a power-law fluid when $\tau_Y = 0$, and to a Newtonian fluid when $n = 1$ and $\tau_Y = 0$. The shear thinning behavior is associated with $0 < n < 1$ and the (less usual) shear thickening behavior with $n > 1$.

C. Viscoelastic (VE) model: Oldroyd

Oldroyd (1950) proposed the following VE model:

$$\frac{\eta}{G}\overset{\nabla}{\tau}+\tau=2\eta D, \tag{7}$$

where $G>0$ is the elastic modulus and η/G is a relaxation time. The total stress is $\sigma=2\eta_2 D+\tau$ where η_2 is a second viscosity, often called the solvent viscosity in the context of polymer solutions. When $\eta_2=0$, the Oldroyd model reduces to the so-called Maxwell model. The upper-convected tensorial derivative $\overset{\nabla}{\tau}$ is defined by

$$\overset{\nabla}{\tau}=\frac{\partial\tau}{\partial t}+\mathbf{v}.\nabla\tau-\tau.\nabla\mathbf{v}^T-\nabla\mathbf{v}.\tau. \tag{8}$$

The dimensionless Weissenberg number is

$$We=\frac{\eta V}{G\,\Delta r}. \tag{9}$$

It compares the characteristic viscous stress $\eta V/\Delta r$ with the elastic modulus G. When $1/G=0$, the Oldroyd model reduces to a Newtonian one.

D. EVP model: Saramito

Saramito (2007, 2009) and Bénito *et al.* (2008) derived (independently) tensorial EVP models that combine viscoelastic and viscoplastic properties (see Fig. 3 and Table I). They satisfy the second law of thermodynamics and match the behavior of nonthixotropic EVP materials such as foams and emulsions: elastic solid before yielding and viscoelastic flow after yielding.

The EVP model presented by Saramito (2009) is simple enough to allow for the numerical resolution (with good convergence, see Appendix B) of the associated partial differential equations even in intricate two- [Cheddadi *et al.* (2011a)] and three-dimensional geometries and is thus suitable for practical and industrial purposes. It is written

$$\frac{1}{2G}\overset{\nabla}{\tau}+\max\left(0,\ \frac{|\tau_d|-\tau_Y}{2K|\tau_d|^n}\right)^{1/n}\tau=D. \tag{10}$$

When $1/G=0$ we obtain the Herschel–Bulkley model, Eq. (3). Conversely, when $n=1$ and $\tau_Y=0$ we obtain the Oldroyd model, Eq. (7). Finally, when both $1/G=0$, $\tau_Y=0$ and $n=1$, the model is Newtonian.

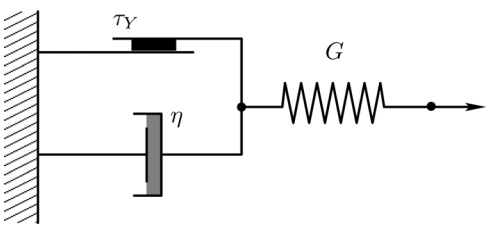

FIG. 3. Schematic representation of the Saramito (2009) EVP model.

In addition to the independent dimensionless numbers (We, Bi, Co, n) already introduced for the Herschel–Bulkley and Oldroyd models, we define the elastic yield strain ε_Y as

$$\varepsilon_Y = \frac{\tau_Y}{2G} = \frac{Bi\,We}{2}. \tag{11}$$

This dimensionless parameter is a measure of the softness and deformability of the material. It has been shown to be the main parameter for the characterization of EVP materials [Cheddadi *et al*. (2011a)] and is often easier to measure from experiments than the yield stress [Marmottant *et al*. (2008)]. The four independent dimensionless numbers (ε_Y, Bi, Co, n) completely characterize the problem (Table II), as do (We, Bi, Co, n).

From now on, the Saramito (2009) model will be referred to as "the EVP model," while the Herschel–Bulkley model will be referred to as "the VP model."

IV. OVERVIEW OF THE EVP MODEL SOLUTIONS

A. Homogeneous flows: Transient response to a simple shear

Saramito (2007, 2009) studied simple flows in a geometry without stress heterogeneity, such as uniaxial extensional flow, oscillating shear flow, or simple shear flow. To enable comparison with the circular Couette geometry (Sec. IV B), we first study the prediction of the EVP model in simple shear flow. The fluid is initially at rest: at $t = 0$, $\tau = 0$. Then, for $t > 0$, a constant shear rate $\dot{\gamma}$ is applied.

The solution $\tau(t)$ is then computed from Eq. (10). As long as there is no stress heterogeneity, the EVP model does not predict any localization. Figures 4(a) and 4(b) plot the normalized shear stress growth coefficient $\eta_S^+ = \tau/\dot{\gamma}$ and the first normal stress difference $N_1 = \tau_{11} - \tau_{22}$ with respect to the applied shear $\dot{\gamma}t$. At first, when the stress in the material is still below the yield stress τ_Y, the shear stress increases *linearly* with time, while the first normal difference increases *quadratically*: the material behaves as an elastic solid obeying the Poynting law [Höhler *et al*. (2004)]. Such a nonlinear phenomenon has been seen experimentally in foams [Labiausse *et al*. (2007)]. After this initial elastic transient, saturation occurs at large applied shear: the stress components tend to a constant value as the applied shear tends to infinity. At the transition to the steady state, one can observe an overshoot of the shear stress that is more pronounced for small values of n.

Figures 4(c) and 4(d) plot the steady shear viscosity $\eta_S = \lim_{t\to\infty} \eta_S^+$ versus We. For $0 < n < 1$, the shear viscosity decreases monotonically, while it tends to a plateau when $n = 1$. Thus, when $n < 1$, the material is shear thinning. Observe that the value of Bi controls the viscosity plateau at small values of We, while it has less influence on the viscosity for large values of We.

In summary, before yielding, the material behaves as a linear elastic solid, while after yielding it is described by a nonlinear viscoelastic model through the power-law index n.

B. Cylindrical Couette geometry: Startup flow

We can now study how the stress heterogeneity due to the cylindrical Couette geometry modifies the simple shear flow presented in Sec. IV A.

Let us consider an EVP material described by Eqs. (1), (2), and (10), initially at rest, i.e., such that $\mathrm{v} = 0$ and $|\tau_d| < \tau_Y$. For $t > 0$, the inner cylinder moves with a velocity $V > 0$ and the flow develops throughout the gap. The initial spatial distribution of stress

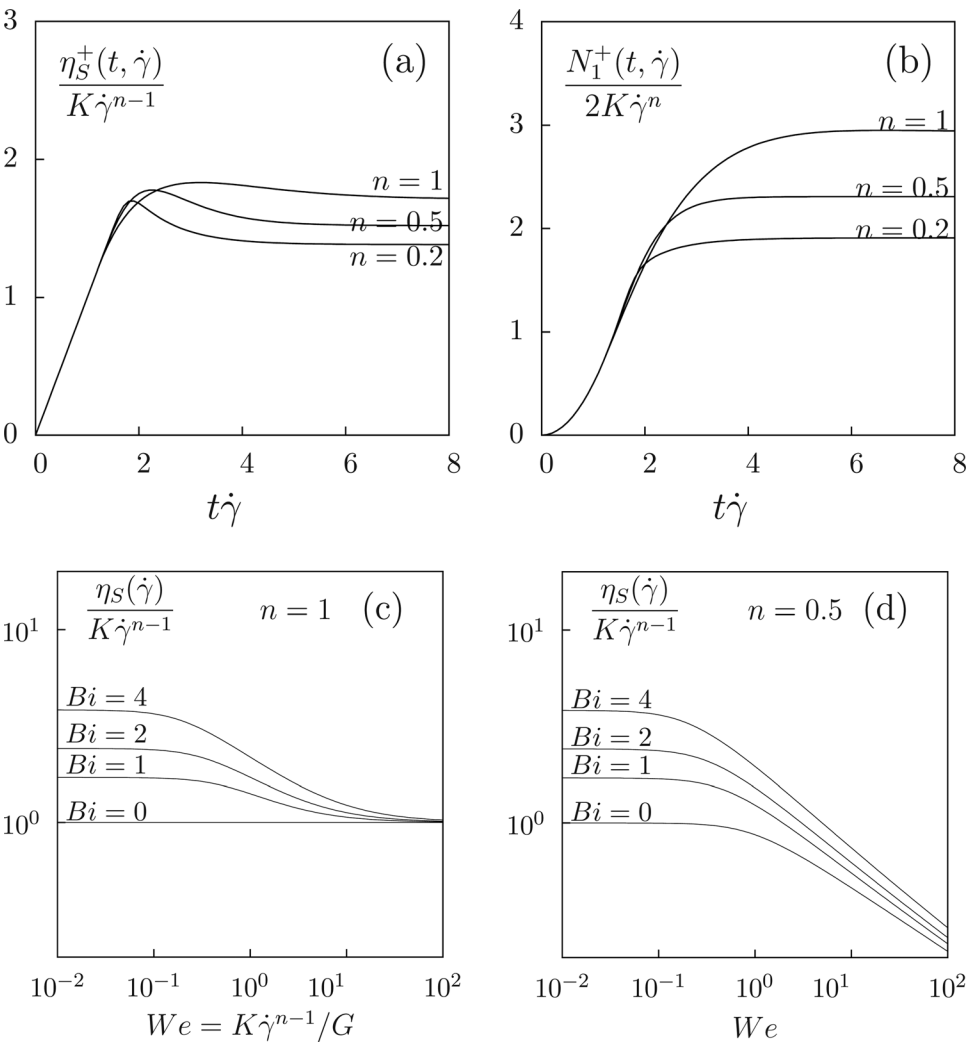

FIG. 4. Start-up shear flow for $We=\eta\dot\gamma/G=K\dot\gamma^{n-1}/G=1$ and $Bi=\tau_Y/(K\dot\gamma^n)=1$: (a) normalized shear stress growth coefficient $\eta_S^+(t,\dot\gamma)$ vs normalized time; (b) normalized first normal stress difference $N_1^+(t,\dot\gamma)$ vs normalized time. Steady shear flow: shear stress coefficient $\eta_S(\dot\gamma)$ vs We for various values of Bi: (c) $n=1$; (d) $n=0.5$.

reflects the preparation of the material [Labiausse *et al*. (2007)]. At first, while $|\tau_d|<\tau_Y$, no plasticity occurs and the equations can be solved explicitly for $n=1$ (Appendix C). The component τ_{rr} is constant and equal to its initial condition, while the shear stress $\tau_{r\theta}(r,t)$ is *linear* in the shear strain

$$\tau_{r\theta}(r,t)=\tau_{r\theta}(r,0)-\frac{G}{2}\frac{1-Co}{Co^2(2-Co)}\left(\frac{\Delta r}{r}\right)^2\frac{Vt}{\Delta r}, \tag{12}$$

and the material develops normal stresses which are *quadratic* in the shear strain

$$\tau_{\theta\theta}(r,t)=\tau_{\theta\theta}(r,0)+\frac{G}{2}\left(\frac{1-Co}{Co^2(2-Co)}\left(\frac{\Delta r}{r}\right)^2\frac{Vt}{\Delta r}\right)^2. \tag{13}$$

Below the yield stress, the material exhibits the same elastic behavior as in simple shear, except for the $1/r^2$ spatial heterogeneity of the shear stress. Because of this heterogeneity, the norm of the deviatoric stress $|\tau_d|$ first reaches the yield stress τ_Y at the inner boundary. The plasticity dissipates the applied deformation and a steady state is rapidly reached, as shown by Cheddadi *et al.* (2008). When no external force such as friction is present, the saturation propagates instantaneously throughout the gap [see Cheddadi *et al.* (2008)]; therefore, the duration of the transient is of the same order of magnitude as the duration of the elastic regime.

C. Cylindrical Couette geometry: Steady-state solutions

We now review some of the new insights gained from the tensorial EVP model, with an emphasis on the differences with scalar and/or VP models. Figure 5 shows all the components of some solutions of the EVP model, for a set of parameters used as reference [Eq. (14) and Fig. 2(b)], and compares them to the VP model. The exploration of these parameters will be presented in Sec. V. We define the critical shear rate $\dot{\gamma}_c$ as the jump of $\dot{\gamma} = 2D_{r\theta}$ at $r = r_c$: it is visible as the slope of the velocity profile [see, for instance, Fig. 5(a)].

1. Range of possible initial conditions

The EVP constitutive equation [Eq. (10)] includes derivatives of the elastic stress tensor with respect to time and, therefore, allows the study of transient flows, as has been done by Cheddadi *et al.* (2008). This in turn requires to specify an initial condition that reflects the preparation of the material before the beginning of the experiment. In particular, the tensorial framework allows us to study various initial normal stresses.

Three different constant values for $\tau_{\theta\theta}$ are chosen. We denote by EVP^0 the case where the components of the initial stress are all set to zero. We then explore two limit cases, in which the component $\tau_{\theta\theta}$ is such that the norm of the initial deviatoric stress tensor is $|\tau_d(r, \theta, t=0)| = \tau_Y$, while the other stress components are zero, $\tau_{r\theta}(r, \theta, t=0) = \tau_{rr}(r, \theta, t=0) = 0$. We thus introduce the two cases $\text{EVP}^{\pm}$ corresponding to initial stresses $\tau_{\theta\theta}(r, \theta, t=0) = \pm\sqrt{2}\tau_Y$. Note that the component $\tau_{rr}(r, \theta, t)$ remains constant and equal to its initial value zero in the cylindrical Couette geometry [see Eq. (10)]. We denote by r_c^+ (resp. r_c^-) the critical radius corresponding to EVP^+ (resp. EVP^-).

2. Results

The results from the EVP model are dramatically different to the results from the VP model, for which the (steady-state) velocity is unique, the normal stress components are zero and the localization length r_c is also unique for a given set of its parameters.

a. Effect of the initial conditions. Surprisingly, Fig. 5 shows that the steady-state solution depends on the initial conditions. We find that they lead to three different steady-state solutions, both for the velocity profile [Fig. 5(a)] and for the stress [Figs. 5(b)–5(d)]. For a given set of parameters (ε_Y, Bi, Co, n), when the initial condition varies the EVP model predicts a *continuous set of steady-state solutions*.

b. Nonuniqueness of the localization length. Depending on the initial condition, the critical radius r_c can reach any value in the range $[r_c^+, r_c^-]$; the highest critical shear rate is reached for the solution with EVP^-. We find that $r_c^+ = r_0 + 0.33\Delta r$ is close to the value predicted by the VP model, but $r_c^- = r_0 + 0.24\Delta r$ is significantly smaller, while the critical radius $r_c^0 = r_0 + 0.28\Delta r$ for EVP^0 is in between.

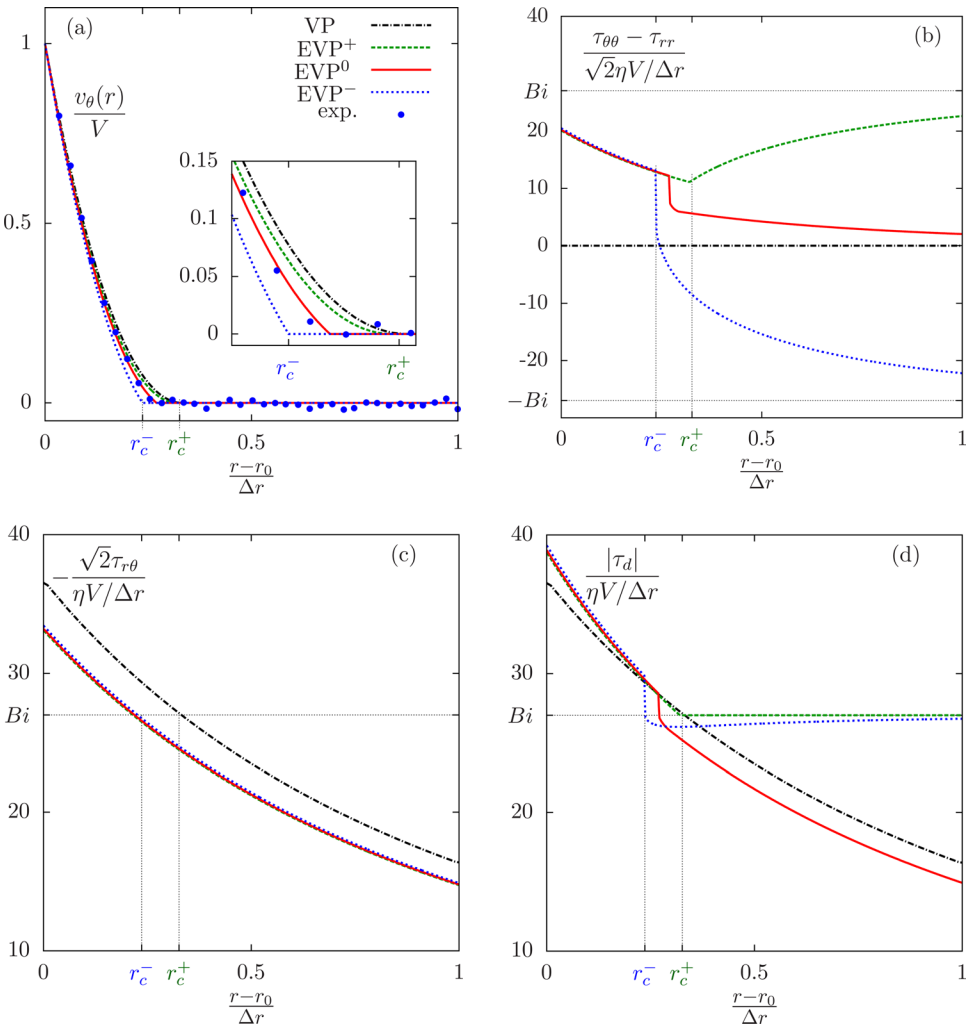

FIG. 5. Comparison between the steady-state solutions of the VP Herschel–Bulkley model and the EVP Saramito model in cylindrical Couette geometry: (a) velocity, with same experimental data as in Fig. 2(b) (Coussot *et al.*, 2002) (b) normal stress; (c) shear stress; (d) norm of the deviatoric stress. Lines: solutions of the EVP model for the reference set of parameters [Eq. (14)]: $\varepsilon_Y = 0.35$, $Bi = 27$, $Co = 1/3$, $n = 1$, as shown in Fig. 2(b), with different initial conditions. Thick solid line (denoted EVP^0): $\tau^0_{\theta\theta} = 0$; thin dashed line (EVP$^+$): $\tau^0_{\theta\theta} = \sqrt{2}\tau_Y$; thin dotted line (EVP$^-$): $\tau^0_{\theta\theta} = -\sqrt{2}\tau_Y$; thick dash-dotted line (VP): $Co = 1/3$, $Bi = 27$, $n = 1$. We denote r_c^+ (resp. r_c^-) the critical radius of the EVP$^+$ (resp. EVP$^-$) solution.

c. Memory effects. Unlike the VP model, the EVP model exhibits nonzero normal stresses [Fig. 5(b)]: in the flowing region ($r < r_c$) where plastic rearrangements occur continuously ($|\tau_d| > \tau_Y$), the normal stress is independent of the initial conditions, and the material progressively loses memory of the initial condition. Conversely, in the nonflowing region ($r > r_c$ and $|\tau_d| < \tau_Y$), the normal stress depends strongly on the initial conditions. The material thus keeps a record of the initial conditions through residual normal stresses.

d. Smooth and nonsmooth solutions. Unlike the VP model, the EVP model can exhibit either smooth (EVP$^+$) or nonsmooth profiles (EVP^0, EVP$^-$): the velocity gradient and the normal stress can be discontinuous at $r = r_c$ [Fig. 5(a)]. Compared to EVP^0,

EVP$^-$ exhibits a stronger localization ($r_c^- < r_c^0$), a higher $\dot{\gamma}_c$, and a higher jump of the normal stress [Fig. 5(b)].

3. Comment on the nonuniqueness of the steady-state solutions

First, we point out that, *for each given initial condition*, the corresponding time-dependent problem is well-posed, its time-dependent solution is unique, and the associated steady-state solution is unique too. Let us then analyze the sources of the nonuniqueness of the solution.

First, from a qualitative point of view, the nonuniqueness of the steady-state solution can be related to the transient elastic regime: in the extreme EVP$^-$ case, the component $\tau_{\theta\theta}$ starts with a negative value that quadratically evolves with time [Eq. (13)]; meanwhile, the shear stress develops throughout the gap [Eq. (12)], and as its contribution to the von Mises criterion dominates that of the normal stresses [see Eq. (4) and Figs. 5(b) and 5(c)], the yield stress value τ_Y is reached, while the normal stresses are still negative. In the flowing region near the inner cylinder, the plastic term is not zero anymore and strongly couples the component of the normal stresses to the flow. Their value is prescribed by the flow and no longer depends on the initial condition in the flowing region [Fig. 5(b)]; it differs from the nonflowing region where the normal stresses profiles strongly depend on the initial condition. When the steady-state regime is reached, these two regions do not join up, which results in discontinuous normal stresses and shear rate. The jump decreases as the initial stress is increased (solutions EVP^0 and EVP$^+$, Fig. 5).

Second, from a formal point of view, the VP model [Eq. (3)] contains one nonlinearity, related to the von Mises criterion. The EVP model [Eq. (10)] adds a second nonlinearity contained in the Oldroyd derivative [Eq. (8)]. Due to the expression of this Oldroyd derivative, the steady-state EVP equations do not reduce to the VP model. The additional term couples the normal stresses components with the shear stress and the velocity gradient (Appendix D). Therefore, even though the velocity gradient reduces here to the shear component, the EVP steady-state solution develops nonzero normal stresses. This additional nonlinearity, interacting with the von Mises criterion, causes nonuniqueness of the stresses in the vicinity of $|\tau_d| = \tau_Y$, i.e., in the vicinity of $r = r_c$.

D. Comparison with experiments

We explain here how the parameters of the EVP model were chosen in order to fit the experimental data shown in Fig. 2.

1. Smooth velocity profiles: The Debrégeas et al. experiment

In the foam experiment shown in Fig. 2(a), image analysis was used to find the steady-state velocity profiles [Debrégeas *et al.* (2001)]; it was reanalyzed by Janiaud and Graner (2005) who measured the shear and normal components of the local elastic strain, in both the transient and steady-state regime.

In the experiment, a steady state is reached after a transient regime. The rotation direction is then inverted, and after a second transient another steady state is reached: this is when measurements are recorded [Debrégeas *et al.* (2001)]. To perform a comparison, we use the experimental steady state as an initial condition, invert the rotation, compute the numerical solution until a first steady state is reached, then again invert the rotation, and compare the corresponding steady state with experiments.

The value of the curvature number is fixed by the geometry,

$$Co = 1 - \frac{r_0}{r_e} = 1 - \frac{71}{122} \approx 0.41803.$$

We have to adjust the value of the three remaining parameters: ε_Y, Bi, n. We focus on the steady-state measurements of elastic strain and velocity.

We start with the yield strain ε_Y; this parameter is independent of the velocity and exerts a large effect on the elastic strain $\varepsilon^{(e)} = \tau_{r\theta}/(2G)$ [see Cheddadi *et al.* (2011b)]. We find that $\varepsilon_Y = 0.175$ allows a good fit of the measured value of the shear elastic strain [Fig. 6(a)]. The initial normal components of the strain are not affected [Fig. 6(b)] by the successive rotations in the region $r > r_c$ and remain below the yield strain ε_Y: this region undergoes reversible elastic deformation.

Then, we have to adjust the values of Bi and n. These parameters have much less effect than ε_Y on the profiles of $\varepsilon^{(e)}$, but they do affect the localization length and the smoothness of the solution (see supplementary material in document E-JORHD2-56-005201. Information on accessing this document is contained at the end of the references). As this experiment exhibits a very smooth transition from the flowing to the nonflowing region (exponentiallike decrease of the velocity), our sensitivity analysis (see Sec. V D) yields a good agreement with the data when using a small value of the power-law index, $n = 1/3$.

The localization length can be measured from the experiment: $r_c - r_0 \approx 0.3\ \Delta r$; we can use this information in the EVP model, taking advantage of the fact that the localization is a VP effect and is mostly determined by the underlying VP model. This last model yields a relation between the values of r_c, Bi, and n [see Appendix A, Eq. (A1)]: with the chosen value of Co and $n = 1/3$, it yields $Bi \approx 7.6$. This value is slightly adjusted in the EVP model in order to improve the fit: we obtain a better fit of the velocity profile with $Bi = 10$.

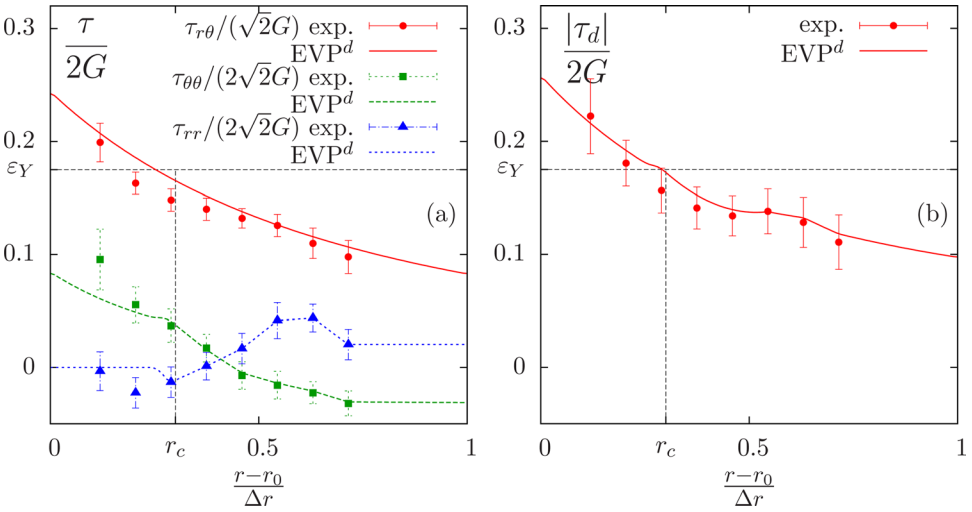

FIG. 6. The stress tensor: comparison of computations and experiments: (a) components; (b) norm of the tensor. Lines: computations with $\varepsilon_Y = 0.175$, $Bi = 10$, $Co = 0.41803$, $n = 1/3$. Symbols: experiments (Debrégeas *et al.*, 2001) analyzed by Janiaud and Graner (2005); errors bars have been provided by Janiaud (private communication).

2. Nonsmooth profiles: The Coussot et al. experiment

The experiment shown in Fig. 2(b) was made with a bentonite-water suspension, using MRI [Coussot *et al.* (2002)]. MRI measurements provide a precise and sharp velocity profile that could not be obtained with foams (Sec. VI A). We use it here to explore the solutions of the EVP model, without claiming to explain the particular properties of bentonite (which is thixotropic) or any other specific material.

For this experiment, only the steady-state velocity has been measured, which makes it more difficult to evaluate precisely the parameters of the EVP model. Since the normal stresses are not measured, we take an initial condition set to zero for the sake of simplicity. As the velocity profile is quite abrupt in the vicinity of $r = r_c$, we choose $n = 1$ for the power-law index. Then, as for the previous experiment, we evaluate the Bingham number Bi under the condition that the critical radius predicted by the underlying VP model matches the value in the experiment ($r_c - r_0 = 0.28\ \Delta r$). From this point, the slope of velocity at $r = r_c$ (which is directly related to the critical shear rate) can be adjusted by tuning the yield strain ε_Y. The best fit is obtained with $\varepsilon_Y = 0.35$ and $Bi = 27$.

V. SENSITIVITY TO THE PARAMETERS

Now, we study how the range $[r_c^-, r_c^+]$ and the critical shear rate $\dot{\gamma}_c$ depend on the parameters of the EVP model. We explore the parameter space with the dimensionless numbers (ε_Y, Bi, Co, n). It allows us to probe the effect of the imposed velocity V, through the Bingham number, as it is the only one that depends on V; the geometry, through the curvature number Co; and the two material parameters: the yield strain ε_Y, and the power-law index n. These parameters are varied around a reference set of parameters used for the comparison with Coussot *et al.* (2002) [Sec. IV D 2, Fig. 2(b)]

$$\varepsilon_Y = 0.35, \quad Bi = 27, \quad n = 1, \quad Co = 1/3. \tag{14}$$

A. Effect of the inner cylinder velocity V

The effect of the imposed velocity V is probed through Bi, which is varied in the range [10, 60] around the reference value $Bi = 27$. If V_0 is the velocity associated with this

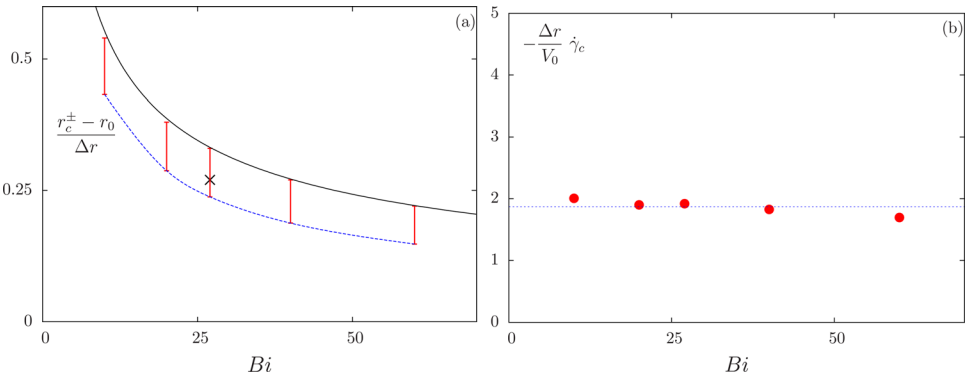

FIG. 7. Effect of the Bingham number Bi. (a) r_c^- and r_c^+. Red bars: five examples of the range in which $(r_c - r_0)/\delta r$ varies. Cross: parameters as Eq. (14) together with $\tau(t=0) = 0$. Solid line: value predicted by the VP model with the same parameters except that $\varepsilon_Y = 0$. From Coussot *et al.* (2002), Fig. 1(a), we get $V_0/\Delta r \approx 6.3\ \mathrm{s}^{-1}$. (b) Corresponding values of $\dot{\gamma}_c$.

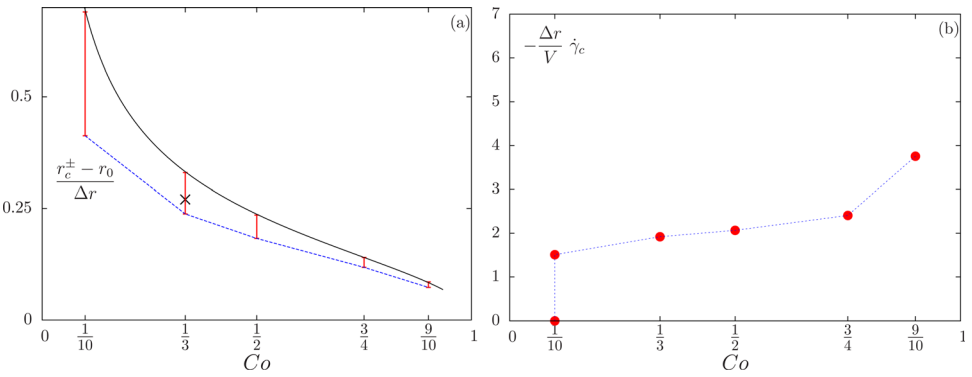

FIG. 8. Effect of the curvature Co: legend as in caption of Fig. 7.

reference value, the range of Bi corresponds roughly to the range $[V_0/3, 3V_0]$ for the velocity. Observe in Fig. 7(a) that when the Bingham number Bi increases then r_c decreases and the size of the zero-velocity zone increases. The critical radius r_c^+ almost matches the critical radius predicted by the VP model. The flow becomes more localized and the gap between r_c^- and r_c^+ also decreases slowly. The marker represents our reference solution [in Fig. 7(a)]. We observe in Fig. 7(b) that $\dot{\gamma}_c$ is almost constant when Bi varies. Varying the velocity affects the size of the zero-velocity zone but has little effect upon the possible abruptness of the solution, nor on the range $[r_c^-, r_c^+]$.

B. Effect of the curvature Co

The curvature number Co explores the effect of the curvature of the geometry. Recall that $Co \to 0$ corresponds to the plane Couette, with a homogeneous stress throughout the gap, while Co close to one corresponds to cylindrical Couette with a tiny central cylinder, and a highly heterogeneous stress. Observe in Fig. 8 that the size of the zero-velocity zone decreases when Co tends to one. The critical radius r_c^+ of the smooth solution is well predicted by the VP model. Note, also, that the difference $r_c^+ - r_c^-$ decreases with Co: thus, when r_c is close to r_0, the effect of the initial condition on the localization length is less visible. Also, the maximal discontinuity $\dot{\gamma}_c$ of the critical shear rate increases with Co.

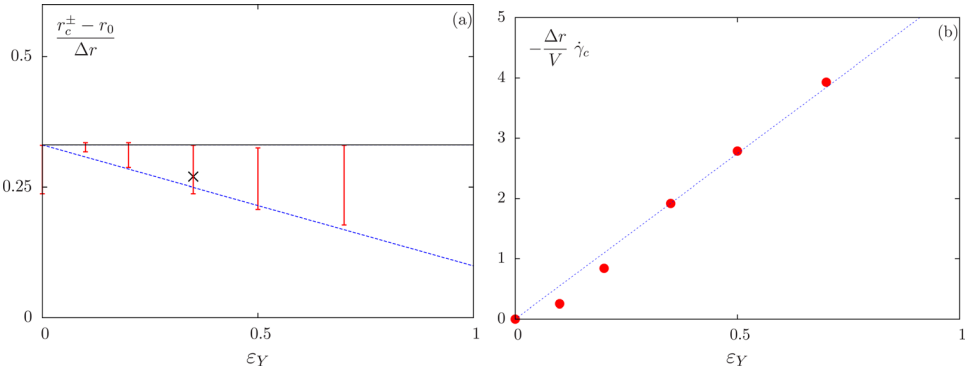

FIG. 9. Effect of the yield strain ε_Y: legend as in caption of Fig. 7. Dashed lines: fits of the EVP$^-$ solutions to the data.

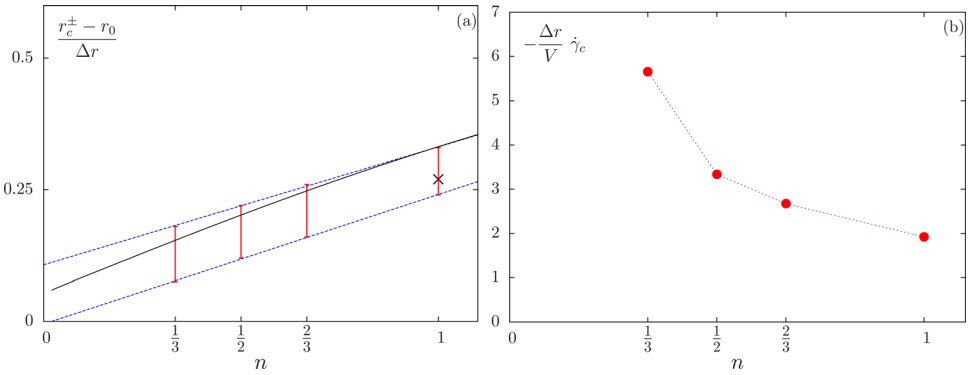

FIG. 10. Effect of the power-law index n: legend as in caption of Fig. 7.

C. Effect of the yield strain ε_Y

The yield strain ε_Y has only a small impact on the EVP$^+$ solution and a large effect on the velocity profile of the EVP$^-$ solution: r_c^- decreases and $\dot{\gamma}_c$ increases, both quasilinearly, when ε_Y increases (Fig. 9). A linear regression through our numerical data leads to

$$\begin{aligned} \frac{r_c^- - r_0}{\Delta r} &\approx -0.23\,\varepsilon_Y + 0.33, \\ -\frac{\Delta r}{V}\dot{\gamma}_c &\approx 5.5\,\varepsilon_Y. \end{aligned} \tag{15}$$

Note that both the range $r_c^+ - r_c^-$ and the discontinuity $\dot{\gamma}_c$ increase with ε_Y. Accordingly, when ε_Y vanishes, $r_c^- = r_c^-$ and $\dot{\gamma}_c = 0$: the solution is unique and smooth: there is no elasticity and the model reduces to the VP one.

D. Effect of the power-law index n

From Fig. 10, the range $r_c^+ - r_c^-$ appears to remain roughly constant, while the size of the yielded zone increases with n. The critical radius r_c^+ decreases with n, as for the VP model. The $\dot{\gamma}_c$ discontinuity of the shear rate for the extreme EVP$^-$ solution decreases with n. These effects are not intuitive.

Another way to explore the effect of n is to vary it, while r_c is held fixed. In fact, the critical radius r_c is approximately given by the VP model and can then be predicted as a function of (Bi, n, Co) (Appendix A). Inverting this function yields $Bi(r_c, n, Co)$: this value of Bi (Table III) is then injected in the EVP model. Using this procedure, the values of n and Bi are varied in such a way that r_c remains constant.

The solutions to the EVP model are represented in Fig. 11. Figure 11(a) shows the EVP$^+$ smooth solution, associated with $r_c^+ \approx r_0 + 0.3\Delta r$, while Fig. 11(b) plots the EVP$^-$ nonsmooth one, with $r_c^- \approx r_0 + 0.23\Delta r$. Note that both r_c^+ and r_c^- are now roughly constant, and that the velocity profile is more curved when n is small.

TABLE III. Effect of the power-law index n while r_c remains fixed: values of n and corresponding values of Bi ($\varepsilon_Y = 0.35$, $Co = 1/3$).

n	1/3	1/2	2/3	1
Bi	9.54785	12.7851	16.6489	27

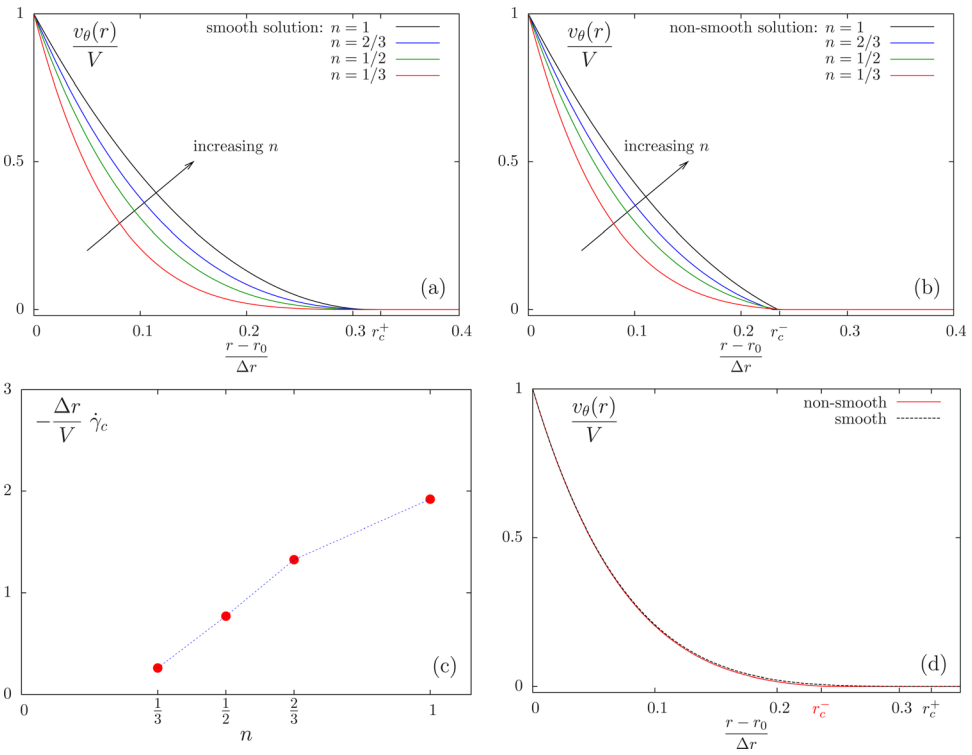

FIG. 11. Effect of the power-law index n at fixed r_c: (a) EVP$^+$ smooth and (b) EVP$^-$ nonsmooth velocity profiles, (c) $\dot{\gamma}_c$; (d) smooth (dashed) and nonsmooth (continuous) profiles for $n = 1/3$.

Figure 11(c) shows $\dot{\gamma}_c$: observe that the discontinuity decreases rapidly when n decreases. For $n = 1/3$, the nonsmoothness becomes imperceptible, while the EVP$^+$ smooth and EVP$^-$ nonsmooth profiles are very close and almost indiscernable, as shown in Fig. 11(d). Note that even when $n = 1/3$, there are still multiple solutions, and the range for r_c remains as large as $[r_c^- - r_0,\ r_c^+ - r_0] \approx [0.23,\ 0.3]\Delta r$, despite the fact that these solutions share similar curved profiles.

VI. DISCUSSION

A. Smooth and nonsmooth profiles

The debate about smooth and nonsmooth velocity profiles, mentioned in the Introduction, is difficult to address experimentally, for two reasons.

First, since the steady-state solution is not unique, both smooth and nonsmooth profiles can be observed in the *same* experiment. This depends on the residual stresses due to the initial preparation, which are usually not reproducible and are certainly difficult to suppress [Labiausse *et al.* (2007); Raufaste *et al.* (2010)], or on the presence of some impurities. This high sensitivity might explain some discrepancies in the literature, and the difficulty to settle the debates regarding localization.

Second, the experiments in foams are not always precise enough to discriminate between smooth and nonsmooth transitions. Figure 12 compares experimental measurements and the two solutions: EVP$^+$, the smooth one, with dashed lines, and EVP$^-$, the nonsmooth one, with solid lines. Experiments were performed with bubble rafts, and in order to reflect the absence of top and bottom plates, the fluid viscosity is introduced in computations as a second Newtonian viscosity η_2 with a viscosity ratio $\alpha = \eta/(\eta + \eta_2)$

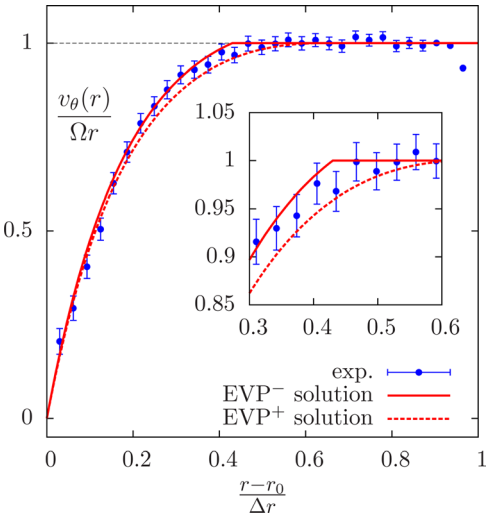

FIG. 12. Foam showing abrupt velocity profile. Comparison of experimental data, from Gilbreth *et al.* (2006), Fig. 1, with model ($\varepsilon_Y = 0.2$, $Bi = 1.3$, $Co = 0.63333$, $n = 1$, $\alpha = 0.2$) for both smooth EVP$^+$ and nonsmooth EVP$^-$ ($\tau_{\theta\theta}(t=0) = \pm\sqrt{2}Bi$) solutions.

[Saramito (2007, 2009)]. In that case, the smooth solution predicts $r_c^+ = r_0 + 0.65\Delta r$ and the nonsmooth one $r_c^- = r_0 + 0.43\Delta r$ together with a critical shear rate $\dot{\gamma}_c = 0.33\, V/\Delta r$. Observe that neither the smooth nor the nonsmooth solutions can be distinguished from the experimental measurements.

B. Is Couette flow suitable for characterizing EVP materials?

1. Flow geometry

We recommend to study flows where residual stresses do not affect the understanding and measurements. Other requirements should include: well-defined boundary conditions; a good separation of scale between the discrete units, the RVE and the global flow scale; the possibility to have a large variation of the control parameters such as velocity (and in foams, liquid fraction, and bubble size dispersity); a variety of measurements providing stringent tests on the EVP model and its parameters. We have shown using experiments and models that a foam flow around an obstacle (Stokes flow) meets these requirements [Cheddadi *et al.* (2011a)].

Couette flows, due to their simple geometry, have a long history of being used to probe the rheology of Newtonian fluids. They are also suitable for complex liquids such as VE or VP materials. However, the present study questions their use in EVP materials, and especially in foams, which are usually excellent model materials to perform in-lab experiments. In fact, in EVP materials, the initial conditions and the preparation method create residual stresses which are difficult to remove and affect the flow, which thus becomes nonunique and poorly controlled. Care is necessary to interpret the results. Future experimental work could try to deepen our understanding of localization and to test our predictions by working in the following two directions.

2. Sample preparation

The control of the sample preparation, and of the initial normal stresses, is important. Obtaining different (although uncontrolled) initial conditions should be reasonably easy by trying different methods to fill the experimental cell.

Choosing these initial stresses is less easy, but possible, for instance, by performing a high velocity preshear in the reverse direction. If the shear rate is high enough so that no localization is observed in the steady-state regime, the normal stresses reach a value larger than $\sqrt{2}\tau_Y$. Whatever the initial loading of the material, it has been irreversibly erased by the plastic rearrangements. After such a preshear, one should observe smooth velocity profiles, with no critical shear rate. We have numerically checked that after such a high velocity preshear the EVP model predicts a smooth solution (similar to EVP^+), even with the EVP^- initial loading that would lead without preshear to a nonsmooth solution.

Suppressing these initial stresses is approximately (but not completely) possible by a careful sample deposition in the experimental cell [Labiausse *et al*. (2007)]. Complete suppression would, for instance, require applying cycles of oscillating strain of amplitude which begins at around twice the yield strain and then gradually decreases to zero [Raufaste *et al*. (2010)]; since these cycles have to be performed in each of the three dimensions, such suppression of initial stress would require a dedicated experiment and is in fact easier in simulations.

Finally, some coarsening materials such as foams become gradually isotropic with time, so that their trapped stresses slowly decrease [Höhler and Cohen-Addad (2005)].

We emphasize the fact that these two last procedures tend to suppress normal stresses and, therefore, correspond to the EVP^0 initial loading and nonsmooth solutions.

3. Measurements of parameters and variables

We recommend to perform local measurements of strain or stress. *In situ* measurement of strain is purely geometric and independent of any knowledge of the sample physics: it can be performed on most systems where the positions of each discrete constituent object is measurable [Graner *et al*. (2008)], which includes two-dimensional foams [Janiaud and Graner (2005); Marmottant *et al*. (2008)] or colloids. *In situ* measurements of stresses are possible with similar methods by measuring the positions of the discrete constituents and having some knowledge of their physical interactions, for instance, in two-dimensional foams [Marmottant *et al*. (2008)], or in birefringent materials by using photoelasticity [Miller *et al*. (1996)].

Model parameters are all measurable in principle. Note that the yield strain or stress requires a tensorial measurement, and thus normal differences components [Labiausse *et al*. (2007)]. Again, local measurements of strain can help in measuring the yield strain directly [Marmottant *et al*. (2008)].

VII. SUMMARY

We solve here a tensorial model for the cylindrical Couette flow of elastic, viscous, plastic materials. We provide an approximate expression for the rheology versus different material parameters. In turn, our predictions are compared with experiments. We show that there is a complex interplay between elasticity, viscosity, and plasticity, which together (but not separately) account for experimental observations. Even in such a simple geometry, the orientational effects are important, so that a tensorial EVP description is necessary to capture many aspects of the physics: reversible elastic deformation (both shear and normal components) below τ_Y, following the Poynting law; memory of the preparation of the material through the initial stress condition, and consequently nonuniqueness of the steady flow and persistent residual normal stresses; possible appearance of nonsmooth solutions. The normal stresses can be interpreted as an intrinsic structure

parameter at the macroscopic level, and therefore independent of the underlying microstructure. These features can be predicted neither by VP models nor by VE models.

We have computed numerically the value of the localization length versus different parameters so that we can guide experimentalists to design experiments that may or may not exhibit such effects: the effects of the initial conditions are more visible, for instance, when ε_Y is large; or when the dissipation exponent n is large; or when the velocity is large, but small enough to allow for a localization within the gap; or when the heterogeneity from the geometry is small, but large enough to allow for a localization within the gap.

Altogether, our results provide a validation of the continuous material description, a determination of EVP material parameters, and an in-depth understanding of their complex rheology. Finally, it appears that the steady Couette flow, which has stimulated so many debates, is neither robust nor unique. Despite its apparent simplicity, it involves numerous parameters, such as the initial conditions for the stress tensor, and is difficult to use in practice. Couette flow experiments could be complemented with flows in other geometries, with a stronger dependence in time and/or space.

ACKNOWLEDGMENTS

The authors warmly thank S. Cox and G. Ovarlez for detailed comments on the manuscript, M. Dennin and E. Janiaud for providing data, S. Cohen-Addad, B. Dollet, and C. Gay for fruitful discussions, the French Groupe de Recherches "Mousses et Emulsions," C. Gay and C. Philippe-Barache for funding the travels for collaborations. F. G. thanks D. Weaire for intense discussions and questions which stimulated this work.

APPENDIX A: HERSCHEL–BULKLEY SOLUTION IN CYLINDRICAL GEOMETRY

When $\varepsilon_Y = 0$ the EVP model reduces to the VP one, and the velocity profile is given by

$$v_\theta(r) = \left(\frac{\sqrt{2}\, r_c^2\, \tau_Y}{K}\right)^{1/n} r \int_r^{r_c} 1/s \left(\frac{1}{s^2} - \frac{1}{r_c^2}\right)^{1/n} \mathrm{d}s.$$

In the case, where the flow is driven by the inner boundary, the critical radius r_c is given by the following expression:

$$\tau_Y = \frac{K}{\sqrt{2}\, r_c^2} \left(\frac{v(r_0)}{r_0 \int_{r_0}^{r_c} \frac{1}{s}\left(\frac{1}{s^2} - \frac{1}{r_c^2}\right)^{1/n} \mathrm{d}s} \right)^n .$$

It expresses also in dimensionless variables

$$Bi = \sqrt{2}\left(\frac{\Delta r}{r_c}\right)^2 \left(\frac{r_0}{\Delta r} \int_{r_0/\Delta r}^{r_c/\Delta r} \frac{1}{s}\left(\frac{1}{s^2} - \left(\frac{\Delta r}{r_c}\right)^2\right)^{1/n} \mathrm{d}s \right)^{-n}, \tag{A1}$$

For fixed values of n and r_c, the corresponding value of Bi for the VP model, denoted as $Bi^{\mathrm{VP}}(n, r_c)$, can be easily computed by using numerical integration. Conversely, for given Bi and n, the value of r_c associated with the VP model, denoted as $r_c^{vp}(n, Bi)$, can be obtained from a small numerical computation [Fig. 13(a)].

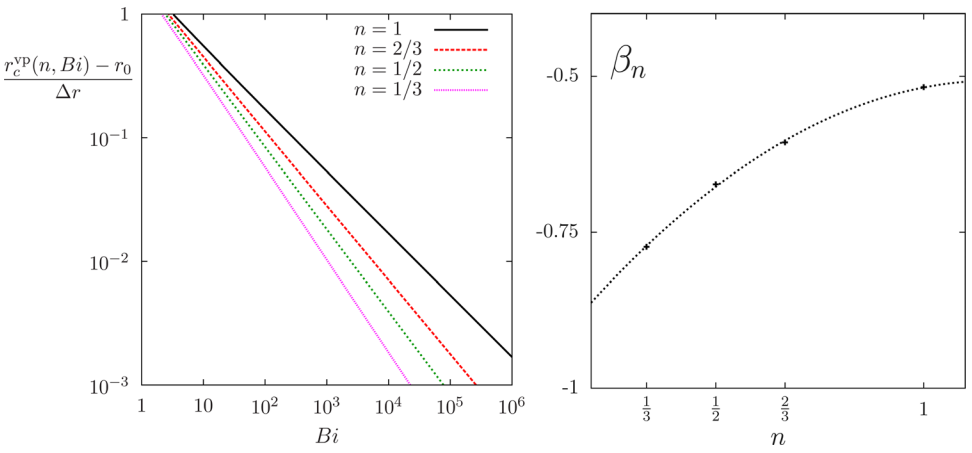

FIG. 13. VP model ($\varepsilon_Y = 0$, $Co = 1/3$): (a) localization versus the Bingham number Bi, for different values of the power-law index n ; (b) index β_n vs n for the power-law $(r_c(Bi,n) - r_0)/\Delta r \approx 1.82 Bi^{\beta_n}$. Dotted line: Eq. (A3).

Figure 13(a) plots r_c as a function of the Bingham number Bi, for $\varepsilon_Y = 0$ (VP model) and $Co = 1/3$, and different values of the power-law index n. Note that the value $Co = 1/3$ corresponds to the geometry of the experiment by Coussot *et al.* (2002) as shown in Fig. 2(b). In this geometry, the localization is observed as long as $r_c/\Delta r < r_e/\Delta r = 1/Co$. The VP model predicts that r_c decreases with the Bingham number: the zero-velocity zone develops and the localization effect is more pronounced. Observe also that the localization effect is more pronounced when n decreases at fixed values of Bi and Co. The r_c value associated with the VP model is denoted as $r_{c,\rm vp}$ (n, Bi) and its inverse function as $Bi_{\rm vp}$ (n, r_c). At fixed n, r_c depends on Bi roughly as a power-law

$$\frac{r_c(Bi,n) - r_0}{\Delta r} \approx 1.82\, Bi^{\beta_n}. \tag{A2}$$

Figure 13(b) represents β_n vs n. A nonlinear regression leads to the dotted line of equation

$$\beta_n \approx -0.38\, n^2 + 0.88\, n - 1.02. \tag{A3}$$

APPENDIX B: NUMERICAL METHOD

The velocity is approximated by continuous affine finite elements, while the stress components are piecewise constant over the mesh. The code is implemented by using the C++ Rheolef finite element library.[1] The stopping criteria for a steady solution are satisfied when the residual term is less than 10^{-8}. Figure 14 shows the convergence versus the mesh size h at the vicinity of $r = r_c$ for the EVP$^-$ nonsmooth steady solution presented in Fig. 5. Observe that the numerical

[1] http://www-ljk.imag.fr/membres/Pierre.Saramito/rheolef/rheolef.pdf.

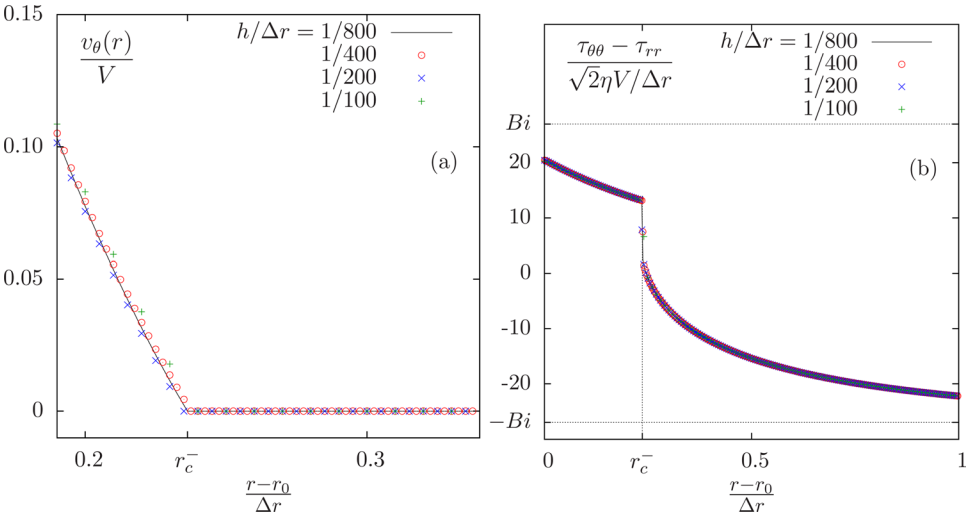

FIG. 14. Convergence vs mesh refinement for the EVP$^-$ nonsmooth solution ($\varepsilon_Y = 0.35$, $Bi = 27$, $Co = 1/3$, $n = 1$) as shown in Fig. 5.

method presents excellent convergence properties, despite the nonsmoothness of the solution: the velocity is nondifferentiable [Fig. 14(a)], while normal stress is discontinuous [Fig. 14(b)].

APPENDIX C: CALCULATIONS FOR STARTUP FLOW

The initial condition is such that $\mathrm{v} = 0$ and $|\tau_d| < \tau_Y$ throughout the gap. For $t > 0$, the inner cylinder moves with a velocity $V > 0$. The calculations that follow are valid as long as no plasticity occurs.

Equation (D5) yields $\tau_{r\theta} = -C(t)/r^2$, where $C(t)$ depends only on time. With $n = 1$, Eq. (D1) yields $\tau_{rr} = 0$ if we choose $\tau_{rr}(r, 0) = 0$ in the initial condition. As a results, Eq. (D2) implies

$$D_{r\theta} = -\frac{C'(t)}{2Gr^2}.$$

Using the fact that $D_{r\theta} = 1/2 \times r\frac{\partial(\mathrm{v}/r)}{\partial r}$, and the boundary conditions $\mathrm{v}(r_0, t) = V$; $\mathrm{v}(r_e, t) = 0$, we find

$$C'(t) = \frac{G}{2}\frac{r_0 r_e^2}{r_e^2 - r_0^2}V,$$

and

$$D_{r\theta} = -\frac{r_0 r_e^2}{r_e^2 - r_0^2}\frac{V}{4r^2} = -\frac{1 - Co}{4Co^2(2 - Co)}\left(\frac{\Delta r}{r}\right)^2\frac{V}{\Delta r}.$$

The expressions (12) and (13) of $\tau_{r\theta}(r, t)$ and $\tau_{\theta\theta}(r, t)$ follow from Eqs. (D2) and (D3).

APPENDIX D: EQUATIONS IN CYLINDRICAL GEOMETRY

The velocity field is $\mathbf{v} = (0, v_\theta, 0)$ in cylindrical (r,θ,z) coordinates. The EVP constitutive equation in cylindrical coordinates writes

$$\frac{1}{2G}\frac{\partial \tau_{rr}}{\partial t} + \max\left(0, \frac{|\tau_d| - \tau_Y}{2K|\tau_d|^n}\right)^{1/n} \tau_{rr} = 0, \tag{D1}$$

$$\frac{1}{2G}\left(\frac{\partial \tau_{r\theta}}{\partial t} - 2D_{r\theta}\tau_{rr}\right) + \max\left(0, \frac{|\tau_d| - \tau_Y}{2K|\tau_d|^n}\right)^{1/n} \tau_{r\theta} = D_{r\theta}, \tag{D2}$$

$$\frac{1}{2G}\left(\frac{\partial \tau_{\theta\theta}}{\partial t} - 4D_{r\theta}\tau_{r\theta}\right) + \max\left(0, \frac{|\tau_d| - \tau_Y}{2K|\tau_d|^n}\right)^{1/n} \tau_{\theta\theta} = 0, \tag{D3}$$

with $|\tau_d| = \left(2\tau_{r\theta}^2 + \frac{1}{2}(\tau_{rr} - \tau_{\theta\theta})^2\right)^{1/2}$. Here, $D = (\bigtriangledown\mathbf{v} + \bigtriangledown\mathbf{v}^T)/2$ is the rate of strain tensor, K denotes a generalized viscosity [Saramito (2009)]. The conservation of momentum writes

$$\frac{\partial p}{\partial r} - \frac{\partial \tau_{rr}}{\partial r} - \frac{\tau_{rr} - \tau_{\theta\theta}}{r} = 0, \tag{D4}$$

$$-\frac{1}{r^2}\frac{\partial}{\partial r}\left(r^2\tau_{r\theta}\right) = 0 \tag{D5}$$

This system of equations is closed by boundary conditions for the velocity at the inner and external cylinders, respectively, $r = r_0$ and $r = r_e$ [Fig. 1(a)], and by initial conditions for both the velocity v_θ and the elastic stress τ.

References

Adams, J. M., and P. D. Olmsted, "Nonmonotonic models are not necessary to obtain shear banding phenomena in entangled polymer solutions," Phys. Rev. Lett. **10**, 067801 (2009).

Barry, J. D., D. Weaire, and S. Hutzler, "Nonlocal effects in the continuum theory of shear localisation in 2D foams," Philos. Mag. Lett. **91**, 432–440 (2011).

Bénito, S., C.-H. Bruneau, T. Colin, C. Gay, and F. Molino, "An elasto-visco-plastic model for immortal foams or emulsions," Eur. Phys. J. E **25**, 225–251 (2008).

Bénito, S., F. Molino, C.-H. Bruneau, T. Colin, and C. Gay, "Shear bands in a continuum model of foams: How a 3D homogeneous material may seem inhomogeneous in 2D," preprint, 2010; e-print arxiv.org/abs/1011.0521.

Berret, J.-F., D. C. Roux, and G. Porte, "Isotropic-to-nematic transition in wormlike micelles under shear," Eur. Phys. J. E **4**, 1261–1279 (1994).

Bingham, E. C., *Fluidity and Plasticity* (McGraw-Hill, New York, 1922).

Cantat, I., S. Cohen-Addad, F. Elias, F. Graner, R. Höhler, O. Pitois, F. Rouyer, and A. Saint-Jalmes, *Les Mousses: Structure et Dynamique* (Belin, Paris, 2010).

Cheddadi, I., P. Saramito, C. Raufaste, P. Marmottant, and F. Graner, "Numerical modelling of foam Couette flows," Eur. Phys. J. E **27**, 123–133 (2008).

Cheddadi, I., P. Saramito, C. Raufaste, P. Marmottant, and F. Graner, "Erratum to numerical modelling of foam Couette flows," Eur. Phys. J. E **28**, 479–480 (2009).

Cheddadi, I., P. Saramito, B. Dollet, C. Raufaste, and F. Graner, "Understanding and predicting viscous, elastic, plastic flows," Eur. Phys. J. E **34**, 11001 (2011a).

Clancy, R. J., E. Janiaud, D. Weaire, and S. Hutzler, "The response of 2D foams to continuous applied shear in a Couette rheometer," Eur. Phys. J. E **21**, 123–132 (2006).

Coussot, P., and G. Ovarlez, "Physical origin of shear-banding in jammed systems," Eur. Phys. J. E **33**, 183–188 (2010).

Coussot, P., J. S. Raynaud, F. Bertrand, P. Moucheront, J. P. Guilbaud, H. T. Huynh, S. Jarny, and D. Lesueur, "Coexistence of liquid and solid phases in flowing soft-glassy materials," Phys. Rev. Lett. **88**, 218301 (2002).

da Cruz, F., F. Chevoir, D. Bonn, and P. Coussot, "Viscosity bifurcation in granular materials, foams, and emulsion," Phys. Rev. E **66**, 051305 (2002).

Debrégeas, G., H. Tabuteau, and J.-M di Meglio, "Deformation and flow of a two-dimensional foam under continuous shear," Phys. Rev. Lett. **87**, 178305 (2001).

Decruppe, J. P., S. Lerouge, and J.-F. Berret, "Insight in shear banding under transient flow," Phys. Rev. E **63**, 022501 (2001).

Denkov, N. D., S. Tcholakova, K. Golemanov, and A. Lips, "Jamming in sheared foams and emulsions, explained by critical instability of the films between neighboring bubbles and drops," Phys. Rev. Lett. **103**, 118302 (2009).

Dennin, M., "Discontinuous jamming transitions in soft materials: Coexistence of flowing and jammed states," J. Phys.: Condens. Matter **20**, 283103 (2008).

Doraiswamy, D., A. N. Mujumdar, I. Tsao, A. N. Beris, S. C. Danforth, and A. B. Metzner, "The Cox-Merz rule extended: A rheological model for concentrated suspensions and other materials with a yield stress," J. Rheol. **35**, 647–685 (1991).

Gilbreth, C., S. Sullivan, and M. Dennin, "Flow transition in two-dimensional foams," Phys. Rev. E **74**, 031401 (2006).

Graner, F., B. Dollet, C. Raufaste, and P. Marmottant, "Discrete rearranging disordered patterns, part I: Robust statistical tools in two or three dimensions," Eur. Phys. J. E **25**, 349–369 (2008).

Herschel, W. H., and T. Bulkley, "Measurement of consistency as applied to rubber-benzene solutions," Proc. Am. Soc. Test. Mater. **26**, 621–633 (1926).

Höhler, R., and S. Cohen-Addad, "Rheology of liquid foam," J. Phys.: Condens. Matter **17**(41), R1041 (2005).

Höhler, R., S. Cohen-Addad, and V. Labiausse, "A constitutive equation describing the nonlinear elastic response of aqueous foams and concentrated emulsions," J. Rheol. **48**, 679–690 (2004).

Howell, D., R. P. Behringer, and C. Veje, "Stress fluctuations in a 2D granular Couette experiment: A continuous transition," Phys. Rev. Lett. **82**, 5241–5244 (1999).

Huang, N., G. Ovarlez, F. Bertrand, S. Rodts, P. Coussot, and D. Bonn, "Flow of wet granular materials," Phys. Rev. Lett. **94**, 028301 (2005).

Huseby, T. W., "Hypothesis on a certain flow instability in polymer melts," Trans. Soc. Rheol. **10**, 181 (1966).

Isayev, A. I., and X. Fan, "Viscoelastic plastic constitutive equation for flow of particle filled polymers," J. Rheol. **34**, 35–54 (1990).

Janiaud, E., and F. Graner, "Foam in a two-dimensional Couette shear: A local measurement of bubble deformation," J. Fluid Mech. **532**, 243–267 (2005).

Janiaud, E., D. Weaire, and S. Hutzler, "Two-dimensional foam rheology with viscous drag," Phys. Rev. Lett. **97**, 038302 (2006).

Kabla, A., J. Scheibert, and G. Debrégeas, "Quasistatic rheology of foams. I. Oscillating strain," J. Fluid Mech. **587**, 23–44 (2007).

Katgert, G., M. E. Möbius, and M. van Hecke, "Rate dependence and role of disorder in linearly sheared two-dimensional foams," Phys. Rev. Lett. **101**, 058301 (2008).

Katgert, G., A. Latka, M. E. Möbius, and M. van Hecke, "Flow in linearly sheared two-dimensional foams: From bubble to bulk scale," Phys. Rev. E **79**, 066318 (2009).

Katgert, G., B. P. Tighe, M. E. Mobius, and M. M. van Hecke, "Couette flow of two-dimensional foams," Europhys. Lett. **90**, 54002 (2010).

Khan, S. A., C. A. Schnepper, and R. C. Armstrong, "Foam rheology: III. Measurement of shear flow properties," J. Rheol. **32**, 69–92 (1988).

Krishan, K., and M. Dennin, "Viscous shear banding in foam," Phys. Rev. E **78**, 051504 (2008).

Labiausse, V., R. Höhler, and S. Cohen-Addad, "Shear induced normal stress differences in aqueous foams," J. Rheol. **51**, 479–492 (2007).

Lauridsen, J., G. Chanan, and M. Dennin, "Velocity profiles in slowly sheared bubble rafts," Phys. Rev. Lett. **93**, 018303 (2004).

Losert, W., L. Bocquet, T. C. Lubensky, and J. P. Gollub, "Particle dynamics in sheared granular matter," Phys. Rev. Lett. **85**, 1428–1431 (2000).

Marmottant, P., C. Raufaste, and F. Graner, "Discrete rearranging disordered patterns, part II: 2D plasticity, elasticity and flow of a foam," Eur. Phys. J. E **25**, 371–384 (2008).

Miller, B., C. O'Hern, and R. P. Behringer, "Stress fluctuations for continuously sheared granular materials," Phys. Rev. Lett. **77**, 3110–3113(1996).

Mueth, D. M., G. F. Debregéas, G. S. Karczmar, P. J. Eng, S. R. Nagel, and H. M. Jaeger, "Signatures of granular microstructure in dense shear flows," Nature **406**, 385–389 (2000).

Okuzono, T., and K. Kawasaki, "Intermittent flow behavior of random foams: A computer experiment on foam rheology," Phys. Rev. E **51**, 1246–1253 (1995).

Oldroyd, J. G., "A rational formulation of the equations of plastic flow for a Bingham fluid," Proc. Cambridge Philos. Soc. **43**, 100–105 (1947).

Oldroyd, J. G., "On the formulation of rheological equations of states," Proc. R. Soc. London, Ser. A, **200**, 523–541 (1950).

Ovarlez, G., S. Rodts, X. Chateau, and P. Coussot, "Phenomenology and physical origin of shear localization and shear banding in complex fluids," Rheol. Acta **48**, 831–844 (2009).

Ovarlez, G., K. Krishan, and S. Cohen-Addad, "Investigation of shear banding in three-dimensional foams," Europhys. Lett. **91**, 68005 (2010).

Porte, G., J.-F. Berret, and J. Harden, "Inhomogeneous flows of complex fluids: Mechanical instability versus non-equilibrium phase transition," Eur. Phys. J. II **7**, 459–472 (1997).

Puzrin, A. M., A. M. Asce, and G. T. Houlsby, "Rate-dependent hyperplasticity with internal functions," J. Eng. Mech. **129**, 252–263 (2003).

Raufaste, C., S. J. Cox, P. Marmottant, and F. Graner, "Discrete rearranging disordered patterns: Prediction of elastic and plastic behavior, and application to two-dimensional foams," Phys. Rev. E **81**, 031404 (2010).

Rodts, S., J. C. Baudez, and P. Coussot, "From discrete to continuum flow in foams," Europhys. Lett. **69**, 636–642 (2005).

Salmon, J.-B., A. Colin, S. Manneville, and F. Molino, "Velocity profiles in shear-banding wormlike micelles," Phys. Rev. Lett. **90**, 228303 (2003a).

Salmon, J.-B., S. Manneville, and A. Colin, "Shear banding in a lyotropic lamellar phase. II. Temporal fluctuations," Phys. Rev. E **68**, 051504 (2003b).

Saramito, P., "A new constitutive equation for elastoviscoplastic fluid flows," J. Non-Newtonian Fluid Mech. **145**, 1–14 (2007).

Saramito, P., "A new elastoviscoplastic model based on the Herschel-Bulkley viscoplasticity," J. Non-Newtonian Fluid Mech. **158**, 154–161 (2009).

Schall, P., and M. van Hecke, "Shear bands in matter with granularity," Annu. Rev. Fluid Mech. **42**, 67–88 (2010).

Schwedoff, T., "La rigidité des liquides," Congrès Int. Physique **1**, 478–486 (1990).

Vermant, J., "Large-scale structures in sheared colloidal dispersions," Curr. Opin. Colloid Interface Sci. **6**, 489–495 (2001).

Wang, Y., K. Krishan, and M. Dennin, "Impact of boundaries on velocity profiles in bubble rafts," Phys. Rev. E **73**, 031401 (2006).

Weaire, D., and S. Hutzler, *The Physics of Foam* (Clarendon Press, Oxford, 1999).

Weaire, D., R. J. Clancy, and S. Hutzler, "A simple analytical theory of localisation in 2D foam rheology," Philos. Mag. Lett. **89**, 294–296 (2009).

Weaire, D., J. D. Barry, and S. Hutzler, "The continuum theory of shear localization in two-dimensional foam," J. Phys.: Condens. Matter **22**, 193101 (2010).

Wyn, A., I. T. Davies, and S. J. Cox, "Simulations of two-dimensional foam rheology: Localization in linear Couette flow and the interaction of settling discs," Eur. Phys. J. E **26**, 81–89 (2008).

See supplementary material at E-JORHD2-56-005201 for details about each parameter's separate effect.